frontiers | Frontiers in Astronomy and Space Sciences

TYPE Original Research
PUBLISHED 17 February 2026
DOI 10.3389/fspas.2026.1750330

OPEN ACCESS

EDITED BY
Zubair Shaikh,
University of Texas at Dallas, United States

REVIEWED BY
M. M. Hasan,
BRAC University, Bangladesh
ZhiQiang Wang,
Nanjing University of Aeronautics and Astronautics, China

*CORRESPONDENCE
S. Ayaz,
syedayaz263@gmail.com
Imran A. Khan,
iali361@gmail.com

RECEIVED 20 November 2025
REVISED 16 January 2026
ACCEPTED 26 January 2026
PUBLISHED 17 February 2026

CITATION
Khan IA, Ayaz S, Shamir M and Khokhar TH (2026) Role of kinetic Alfvén waves in the non-extensive anisotropic earth's magnetospheric plasma.
Front. Astron. Space Sci. 13:1750330.
doi: 10.3389/fspas.2026.1750330

Role of kinetic Alfvén waves in the non-extensive anisotropic earth's magnetospheric plasma

Imran A. Khan[1,2]*, S. Ayaz[3]*, M. Shamir[4] and Tajammal H. Khokhar[5]

[1]Department of Space Science, Institute of Space Technology, Islamabad, Pakistan, [2]Space and Astrophysics Research Lab (SARL), National Center of GIS and Space Applications (NCGSA), Islamabad, Pakistan, [3]Department of Space Science and CSPAR, University of Alabama in Huntsville, Huntsville, AL, United States, [4]Department of Physics, Faculty of Science and Technology, Thammasat University, Pathum Thani, Thailand, [5]School of Natural Sciences, Department of Physics and Astronomy, National University of Sciences and Technology (NUST), Islamabad, Pakistan

Kinetic Alfvén waves (KAWs) contribute significantly to particle acceleration in the magnetosphere of Earth. In this paper, we discussed how the charged particles' (electrons and ions) speeds vary with distance during the wave-particle interaction. We employed the temperature-anisotropic non-extensive distribution function to model the magnetospheric plasma. Our findings show that the charged particles take more energy from the wave in the non-extensive state; consequently, the particles are accelerated to higher velocities. Our results also show that when the perpendicular ion temperature ($T_{\perp i}$) of the system increases, the accelerated charges have a lower velocity. In addition to the velocity of charged particles, we found that the magnitude of the KAW's group velocity was larger in the Maxwellian ($q \rightarrow 1$) case, and the waves were more energetic and heat the magnetospheric plasma for larger distances. Finally, we calculated the characteristic length scale over which the waves get damped. Our findings show that the damping scale length is of the order of several Earth radii (R_E), consistent with observations. The effects of q and the temperature anisotropy on the damping scale length are such that for small q (i.e., the non-extensive state), and larger $T_{\perp i}$, the damping scale length becomes large enough, which implies that the waves can interact with the charged particles far away from the locations where they are excited. The findings of this study help us understand the formation of the beams of charged particles, which can precipitate into different regions of the magnetosphere, and are critically important in the formation of auroras.

KEYWORDS

damping length, group velocity, kinetic Alfvén waves, magnetospheric plasma, poynting vector, temperature anisotropic non-extensive distribution function

1 Introduction

The magnetosphere of Earth, dominated by the terrestrial magnetic field, shapes the surrounding environment and influences plasma behavior (Wright et al., 2024). The magnetosphere's complex structure of magnetic fields and plasma distributions creates natural coupling opportunities between different wave modes. This coupling, particularly between fast magnetoacoustic and Alfvén modes Alfvén (1942), is integral to magneto-seismology studies, enabling researchers to probe the

magnetospheric dynamics and its responses to solar wind interactions. Alfvén waves are frequently generated when there are unstable particle distributions, and they play a crucial role in driving interactions that impact both the ionosphere and ground-level currents, with significant implications for space weather phenomena (Wright et al., 2024).

Recent advances have expanded the understanding of these waves and the mechanisms by which they accelerate particles within the magnetosphere (Wright et al., 2024). The Earth's magnetosphere hosts a wide range of plasma waves (Walker, 2013), among which Alfvén waves on a microscopic scale, also called KAWs, are particularly important due to their influence on wave-particle interactions in the magnetospheric regions (Gershman et al., 2017). KAWs are characterized by their low-frequency nature (relative to the ion gyrofrequency) and their ability to develop an electric field component parallel to the background magnetic field (Hasegawa and Chen, 1975). When these waves propagate through plasma and interact resonantly with the charged particles, i.e., their parallel phase velocity $\omega_r/k_\parallel$ approach the velocities of the particles moving along the wave, the electric field of the KAWs accelerates the charged particles (Lysak and Song, 2003)

KAWs can propagate over extensive distances within the Earth's magnetosphere, facilitating energy transfer across wide spatial regions (Sharma Pyakurel et al., 2018). Spacecraft observations have shown that within the plasma sheet boundary layer, approximately 10% of the wave energy is transferred to particles over distances ranging from 1.5 to 15 Earth radii (R_E) (Lysak and Song, 2003). This significant energy transfer implies that KAWs have the potential to fully dissipate through resonant interactions with particles if they propagate far enough from their initial generation points. For KAWs to effectively dissipate their energy, they must reach regions well beyond their source locations, where interactions with particles continue to absorb wave energy over vast distances. A comprehensive analysis of these waves can be found in the following studies: (Ayaz et al., 2024a; Ayaz et al., 2024b, Ayaz et al., 2025a; Ayaz et al., 2025b; Cramer, 2011; Wu and Chen, 2020; Keiling, 2024).

KAWs are prevalent across the magnetosphere and are generated through various mechanisms. One prominent mechanism of energy transfer is turbulent cascade (Kolmogorov, 1941). Observations have confirmed the turbulent cascades in the plasma sheet region (Borovsky and Funsten, 2003). A secondary mechanism, ionospheric feedback, contributes to energy transfer on smaller scales. Initially introduced by Atkinson (1970), this feedback mechanism includes the response of the magnetosphere characterized by a field line impedance (Miura and Sato, 1980). Other studies examined the feedback instability in the presence of the field line resonances (Streltsov and Lotko, 2004; Lu et al., 2007; Watanabe, 2014), enhancing our understanding of KAW generation in magnetospheric structures.

Phase mixing also contributes significantly to KAWs generation in the plasma sheet boundary layer (Lysak, 2023). Observations from the Polar satellite showed KAWs activity at 4–6 R_E (Wygant et al., 2002), during which electrons were accelerated in the direction of the parallel electric field of the wave (Lysak and Song, 2011). These findings matched the **E**/**B** ratios predicted by dispersion relations, which allowed for estimates of perpendicular wavelengths and plasma beta, illustrating how phase mixing can sustain KAWs in high-gradient regions.

Additionally, fluctuations in solar wind flow near the magnetopause can excite magnetohydrodynamic waves, which may convert into KAWs (Lee et al., 1994). Velocity-sheared flows further contribute to this process (Wang et al., 1998), as does magnetic reconnection, a major driver of wave production. During reconnection at the magnetopause, KAWs travel along separatrices towards the ionosphere, and substorms in the plasma sheet tail can also generate KAWs through direct reconnection (Shay et al., 2011; Sharma Pyakurel et al., 2018). However, due to their small perpendicular wavelengths, KAWs are susceptible to Landau damping, which can dissipate the waves before reaching the ionosphere. Observations by the MMS mission in December 2015 confirmed KAW presence during reconnection at the dayside magnetopause, underscoring their influence on geomagnetic storm activity and space weather (Gershman et al., 2017; Dai et al., 2023).

On spatial scales larger than several Earth radii, varying numbers of resonant particles engage with waves across different magnetospheric locations, with particle interactions significantly influenced by temperature variations (Khan et al., 2020). Spacecraft observations and simulation results consistently show that magnetospheric temperatures are anisotropic. Near the subsolar magnetopause, the ion perpendicular temperature exceeds the ion parallel temperature (Olson and Lee, 1983), likely due to shock waves generated ahead of tangential discontinuities at the magnetopause (Mandt and Lee, 1991). In the plasma depletion layer, IMP-6 satellite data reveal this same anisotropic pattern ($T_{\perp i} > T_{\parallel i}$), which is associated with plasma flowing along flux tubes (Crooker et al., 1979). The Magnetospheric Multiscale (MMS) mission further confirms this trend in the dayside magnetopause, attributing it to the monochromatic ion cyclotron waves (Gershman et al., 2017).

In addition to anisotropic ion temperatures, these magnetospheric regions show similar anisotropies in electron temperatures. The THEMIS mission's data at the subsolar magnetopause indicate that perpendicular electron temperature exceeds parallel electron temperature, potentially due to magnetic reconnection processes (Tang et al., 2013). This complex temperature structure highlights the particle-wave interactions' dynamic and varied nature across the magnetosphere.

Beyond temperature variations, the non-Maxwellian characteristics of magnetospheric plasma also play a role in determining the number of resonant particles that interact with waves (Khan et al., 2019b; a). The pioneering IMP-1 spacecraft's data revealed that the magnetosphere contains a significant population of suprathermal particles that fit a power-law distribution instead of the traditional Maxwellian distribution (Olbert, 1968). This discovery was later corroborated by various spacecraft, including Orbiting Geophysical Observatory missions OGO 1 and OGO 3 (Vasyliunas, 1968), the Polar spacecraft (Kletzing et al., 2003), International Sun-Earth Explorer-1 (ISEE-1) (Christon et al., 1988; Christon et al., 1991), Magnetospheric Multiscale (MMS) (Pollock et al., 2018), and THEMIS (Kirpichev et al., 2015).

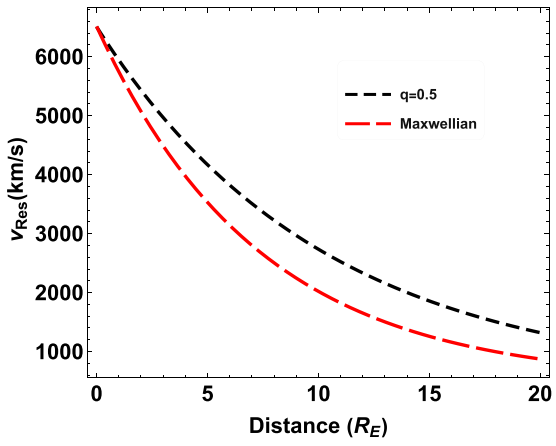

FIGURE 1
Resonant velocity of charged particles. The resonant velocity is calculated using Equation 9, where $n_0 = 10$ cm^{-3}, $B_0 = 55$ nT, $k_\perp = 10^{-7}$ cm^{-1}, and $k_\parallel = 10^{-8}$ cm^{-1}. This figure shows the variation of resonant velocity as a function of distance for $q = 0.5$ and $q \to 1$. The values of the temperatures are fixed: $T_{\parallel e} = T_{\perp e} = 35$ eV, $T_{\parallel i} = 175$ eV, and $T_{\perp i} = 350$ eV, respectively.

A particularly effective model for describing suprathermal particles is the non-extensive distribution function, frequently employed in studies of magnetospheric plasmas (Khan et al., 2019b; Liu et al., 2016; Shamir et al., 2022) and grounded in strong theoretical foundations (Tsallis, 1988). This function provides a robust framework for capturing the effects of suprathermal particles and has proven instrumental in understanding wave-particle interactions in magnetospheric environments.

Inspired by observations of power-law distributions, temperature anisotropies, and KAWs, this study investigates the dynamics of KAWs propagating through the Earth's magnetosphere, modeled with a temperature-anisotropic, non-extensive velocity distribution function. Specifically, we analyze how these waves accelerate charged particles through resonant interactions and examine the influence of the non-extensive q parameter and temperature anisotropy on the energy flow velocity. In addition, we determine the characteristic scale length over which the waves undergo damping and evaluate for different temperature anisotropies and q values. To our knowledge, this research is the first to explore the role of these waves in accelerating charged particles in the Earth's magnetospheric plasma. The mathematical framework supporting these analyses is detailed in the following section.

2 Mathematical model

The geometry of the system is considered in such a manner that the background magnetic field is oriented parallel to the z-axis, the perturbed magnetic field of the wave is directed along the y-axis, and the perturbed electric field of the wave and the wave vector lie the x-z plane.

In the magnetospheric plasmas, across the background magnetic field, KAWs carry a small amount of energy. The energy is predominantly carried by the waves along the background magnetic field (Lysak and Song, 2003). The transport of the energy with respect to distance is governed by the steady-state Poynting theorem, which for the KAWs simplifies to Lysak and Song (2003), Khan et al. (2020), and Xunaira et al. (2023)

$$\frac{\partial S}{\partial z} = \frac{2\omega_r \omega_i}{v_A^2 k_\parallel} S, \tag{1}$$

where S represents the time-averaged Poynting vector, $k_\parallel$ represents the parallel wavenumber, and v_A represents the Alfvén speed. The ω_r (real frequency) and ω_i (imaginary frequency) in the low-β, temperature anisotropic non-extensive distributed plasma can be found by solving the following determinant (Lysak and Song, 2003; Ayaz et al., 2020; Ayaz et al., 2024a):

$$\begin{pmatrix} \epsilon_\perp - k_\parallel^2 c^2/\omega^2 & k_\perp k_\parallel c^2/\omega^2 \\ k_\perp k_\parallel c^2/\omega^2 & \epsilon_\parallel - k_\perp^2 c^2/\omega^2 \end{pmatrix} = 0, \tag{2}$$

where $k_\perp$ represents the perpendicular component of the wavenumber and c represents the light speed. The expressions for $\epsilon_\perp$ and $\epsilon_\parallel$ are (Summers et al., 1994)

$$\epsilon_\perp = 1 + \sum_\alpha \frac{\omega_{p\alpha}^2}{\omega} \int v_\perp d^3v \sum_{n=-\infty}^{n=\infty} \frac{n^2}{\zeta^2} J_n^2(\zeta) \times \left[\left(1 - \frac{k_\parallel v_\parallel}{\omega}\right) \frac{\partial f_{0\alpha}}{\partial v_\perp} + \frac{k_\parallel v_\perp}{\omega} \frac{\partial f_{0\alpha}}{\partial v_\parallel} \right] \Big/ \left(\omega - k_\parallel v_\parallel - n\Omega_\alpha\right), \tag{3}$$

and

$$\epsilon_\parallel = 1 + \sum_\alpha \frac{\omega_{p\alpha}^2}{\omega} \int v_\perp d^3v \sum_{n=-\infty}^{n=\infty} \frac{v_\parallel}{v_\perp} J_n^2(\zeta) \times \left[\frac{n\Omega_\alpha}{\omega} \frac{v_\parallel}{v_\perp} \frac{\partial f_{0\alpha}}{\partial v_\perp} + \left(1 - \frac{n\Omega_\alpha}{\omega}\right) \frac{\partial f_{0\alpha}}{\partial v_\parallel} \right] \Big/ \left(\omega - k_\parallel v_\parallel - n\Omega_\alpha\right). \tag{4}$$

In Equations 3 and 4, $f_{0\alpha}$ is arbitrary velocity distribution function, α is the species under consideration (i.e., electrons/ions), $J_n(\zeta)$ is the Bessel function, ζ is dimensionless quantity given by $\zeta = k_\perp v_\perp / \Omega_\alpha$, where Ω_α is gyrofrequency given by $\Omega_\alpha = q_\alpha B_0 / m_\alpha$, and $\omega_{p\alpha}$ is plasma frequency given by $\omega_{p\alpha} = \sqrt{n_0 q_\alpha^2 / \epsilon_0 m_\alpha}$. All other symbols have their usual meaning.

In the current paper, we chose the following anisotropic non-extensive distribution function (Qiu and Liu, 2013):

$$f_{0\alpha} = A_q \left[1 - (q-1) \left(\frac{v_\perp^2}{\theta_{\perp\alpha}^2} + \frac{v_\parallel^2}{\theta_{\parallel\alpha}^2} \right) \right]^{\frac{2-q}{q-1}}, \tag{5}$$

where

$$A_q = \frac{\sqrt{1-q}\,\Gamma\left(\frac{1}{1-q}\right)}{\pi^{\frac{3}{2}} \theta_{\perp\alpha}^2 \theta_{\parallel\alpha} \Gamma\left(\frac{1}{1-q} - \frac{1}{2}\right)},$$

and $\theta_{\perp,\parallel\alpha} = \sqrt{(3q-1)T_{\perp,\parallel}/2m_\alpha}$. The values of q are restricted to $-1 < q \leq 1$. Putting Equation 5 in Equations 3 and 4 and then following the approach adopted in many studies (see Refs:

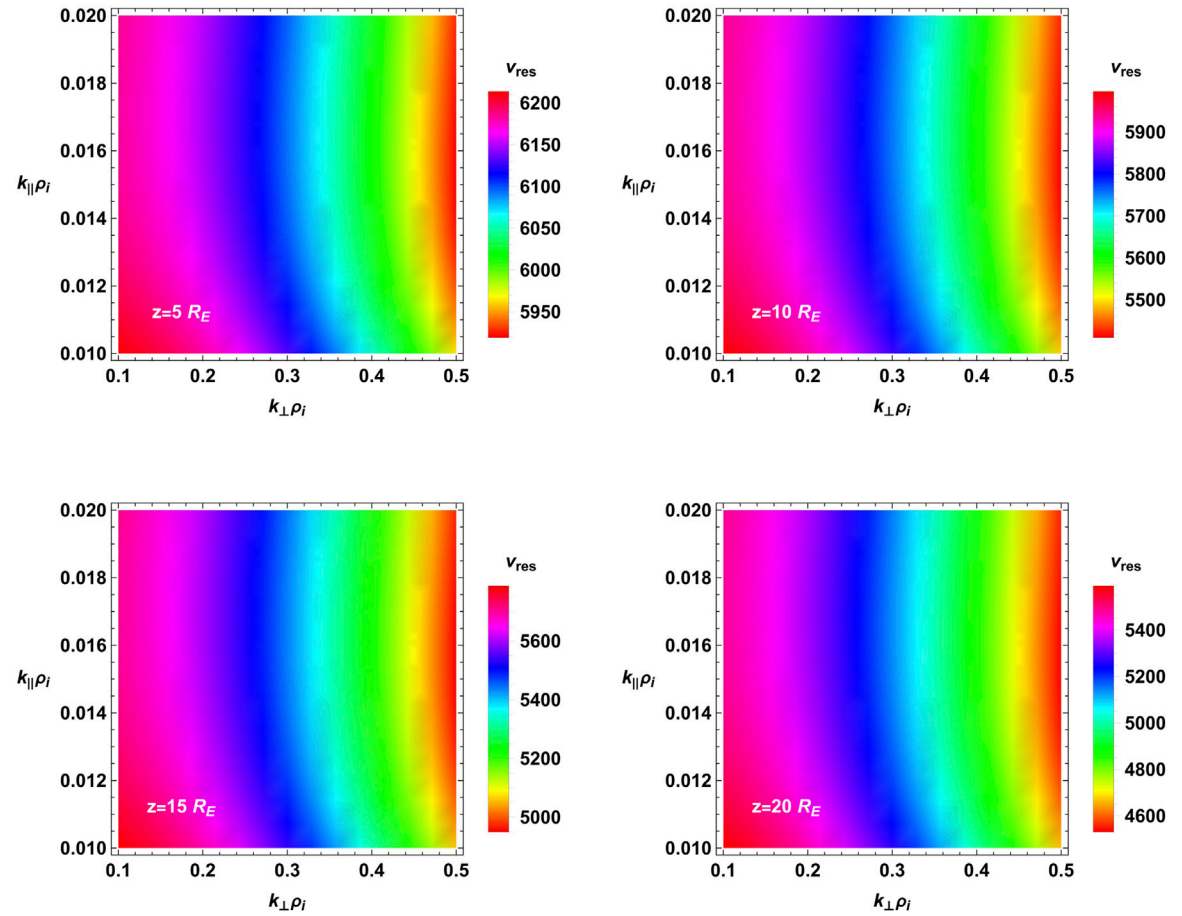

FIGURE 2
Effect of varying wavenumber on the resonant velocity of charged particles. The figures are generated using Equation 9. Both the perpendicular and parallel wavenumbers are normalized with ρ_i. The value of q is 0.5 and all other parameters have the same values as in Figure 1. In the panels, the influence of the wavenumber has been checked at different locations. The bar legends right to the panels (top)–(bottom) represent the magnitude of the resonant velocity. It can be seen that the magnitudes of the resonant speed decrease when z is large.

Lysak and Song (2003); Khan et al. (2020); Ayaz et al. (2025a) and references therein), the $\epsilon_{\perp}$ and $\epsilon_{\|}$ expressions turn out to be

$$\epsilon_{\perp} = \frac{c^2}{v_A^2}\left(1 - \frac{3}{4}\frac{2}{3q-1}\,k_{\perp}^2\,\rho_{iq}^2\right) - \frac{c^2 k_{\|}^2}{\omega^2}\frac{c_{sq}^2}{v_A^2}\psi_1,$$

and

$$\epsilon_{\|} = \frac{2\omega_{pe}^2}{k_{\|}^2\,\theta_{\|e}^2}\left(\frac{1+q}{2}\right) - \frac{\omega_{pi}^2}{\omega^2}\left(1 - k_{\perp}^2\,\rho_{iq}^2\psi_2\right) + 2i\pi\sqrt{1-q}\,\frac{\Gamma\left[1/(1-q)\right]}{\Gamma\left[(1+q)/(2-2q)\right]}\frac{\omega_{pe}^2\omega}{k_{\|}^3\theta_{\|e}^3} \left\{1 + \left(\frac{T_{\|e}}{T_{\|i}}\right)^{3/2}\sqrt{\frac{m_i}{m_e}}\left[1-(q-1)\,\xi_{0i}^2\right]^{\frac{2-q}{q-1}}\right\}.$$

Solving the determinant Equation 2 using the methods employed in Refs: Lysak and Song (2003); Khan et al. (2020); Xunaira et al. (2023); Ayaz et al. (2025a) and references therein, we get the following expressions of ω_r and ω_i:

$$\omega_r^2 = k_{\|}^2 {v_A}^2\left\{\left(1 + \frac{3}{4}\frac{2}{3q-1}\,k_{\perp}^2\,\rho_{iq}^2\right)\left[1 + \frac{c_{sq}^2}{v_A^2}\psi_1\right] + \frac{2}{(1+q)}\frac{T_{\|e}}{T_{\perp i}}\,k_{\perp}^2\,\rho_{iq}^2 + \frac{c_{sq}^2}{v_A^2}\frac{2\left(1-k_{\perp}^2\,\rho_{iq}^2\psi_2\right)}{1+q}\right\}, \tag{6}$$

and

$$\omega_i = -i\pi\frac{\sqrt{1-q}\,\Gamma\left[1/(1-q)\right]}{\Gamma\left[(1+q)/(2-2q)\right]}\left[\left(1 + \frac{c_{sq}^2}{v_A^2}\psi_1\right) + \frac{2}{(1+q)}\frac{T_{\|e}}{T_{\perp i}}\,k_{\perp}^2\,\rho_{iq}^2\right]^{-1} \times \frac{k_{\|}v_A}{1+q}\frac{v_A}{\theta_{\|e}}\left(\frac{2}{(1+q)}\frac{T_{\|e}}{T_{\perp i}}\,k_{\perp}^2\,\rho_{iq}^2 + \frac{2c_{sq}^2}{{v_A}^2}\frac{\left(1-k_{\perp}^2\,\rho_{iq}^2\psi_2\right)}{1+q}\right) \times \left\{1 + \left(\frac{T_{\|e}}{T_{\|i}}\right)^{3/2}\sqrt{\frac{m_i}{m_e}}\left[1-(q-1)\,\xi_{0i}^2\right]^{\frac{2-q}{q-1}}\right\}. \tag{7}$$

In Equations 6 and 7, $\rho_{iq}\left(=\theta_{\perp i}/\sqrt{2}\,\Omega_i\right)$ represents ion gyroradius and $c_{sq} = \sqrt{(3q-1)\,T_{\|e}/2m_i}$ represents sound speed in the non-extensive distributed plasma. Moreover, the temperature

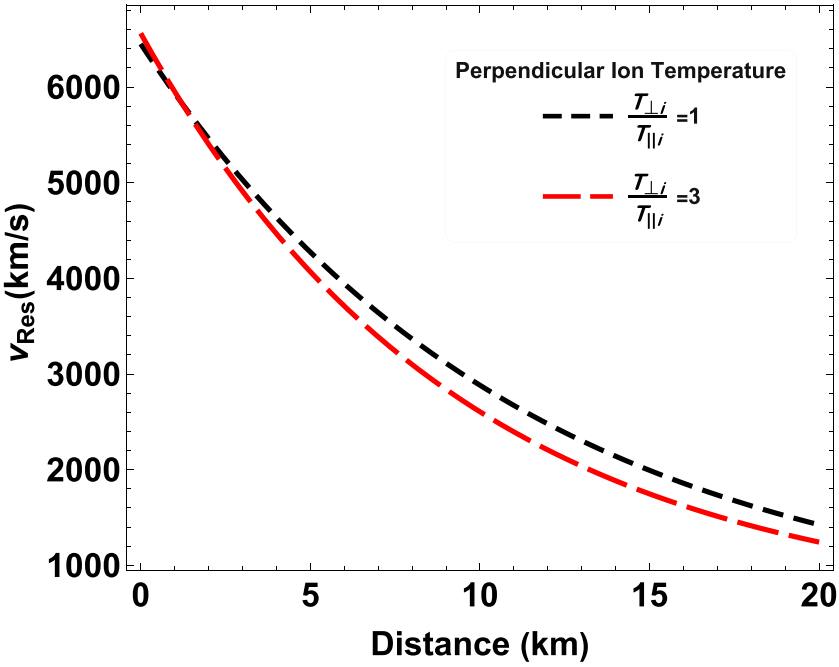

FIGURE 3
Effect of perpendicular ion temperature ($T_{\perp i}$) on the resonant velocity of charged particles. This figure is also based on Equation 9 where q is 0.5 and $T_{\perp i}$ is considered to have different values. The other quantities have the same values as in Figure 1. We can see that when $T_{\perp i}$ increases, the resonant velocity decreases.

anisotropic terms (ψ_1 and ψ_2) in expressions Equations 6 and 7 are defined by the following expressions:

$$\psi_1 = \frac{2}{3q-1}\left[\left(\frac{T_{\perp i}}{T_{\|i}}-1\right)\left(\frac{T_{\|i}}{T_{\|e}}\right)+\left(\frac{T_{\perp e}}{T_{\|e}}-1\right)\right],$$

and

$$\psi_2 = \frac{2}{3q-1}\left[\left(\frac{T_{\|i}}{T_{\perp i}}-1\right)+\left(\frac{T_{\|e}}{T_{\perp e}}-1\right)\frac{T_{\perp e}}{T_{\perp i}}\right].$$

It should be noted that the above expressions are different from the expressions reported in Liu et al. (2016). In that paper, the functional form of the distribution (Equation 1 of Liu et al. (2016)) is different from our Equation 5. Moreover, when $q \to 1$, and $T_{\perp e,i} = T_{\|e,i}$, Maxwellian results can be retrieved (Lysak and Song, 2003), and in the limit, $q \to 1 - 1/\kappa$, the results of Kappa distributed plasma can be retrieved (Khan et al., 2020).

To see how the Poynting vector varies with distance, we have to solve Equation 1, which is a simple first-order differential equation that has the following solution (Khan et al., 2020):

$$S(z) = S(0)\exp\left(\frac{2\omega_r\omega_i}{v_A^2 k_\|}z\right). \tag{8}$$

Expression Equation 8 is valid for studying energy transfer through the Landau damping rate—resonant interaction. When there is no resonant interaction ($\omega_i = 0$), the waves travel undamped, i.e., S(z) = S(0) for all z, where S(0) is the energy per unit area per unit time at the position where the waves are generated.

The resonant particles experience acceleration as a result of taking energy from the wave. If the wave loses energy only through the Landau mechanism, then the average speed of the particles will be (Ayaz et al., 2024b; Ayaz et al., 2025b)

$$v_{res} \approx \frac{\omega_r}{k_\|} + \left(\frac{2S}{\delta}\right)^{1/3}, \tag{9}$$

where δ represents mass density.

During the resonant interaction, the perturbations are supposed not to be very large, so we can assume linear analysis. Considering linear analysis, in Equation 8, the relationship between the Poynting vector and group velocity is not shown explicitly, as we have adopted the model of Lysak and Song (2003). Following the procedure of Bers (1999), the explicit relationship is

$$v_g = \frac{\partial\omega_r}{\partial k} = \frac{S(z)}{w_k}, \tag{10}$$

where w_k represents time-averaged wave energy density. Equation 10 provides information as to how the electromagnetic energy is propagated by the KAWs having different wavelengths.

When the different waves interact with the plasma, the characteristic scale length L over which the wave damps out can be found in terms of the group velocity and damping rate (Tiwari et al., 2008):

$$L = \frac{v_g}{\omega_i}. \tag{11}$$

The above damping length L (i.e., Equation 11) together with the energy flow velocity (given by Equation 10), and the velocity of the resonant particle (given by Equation 9) are graphically analyzed in the next section.

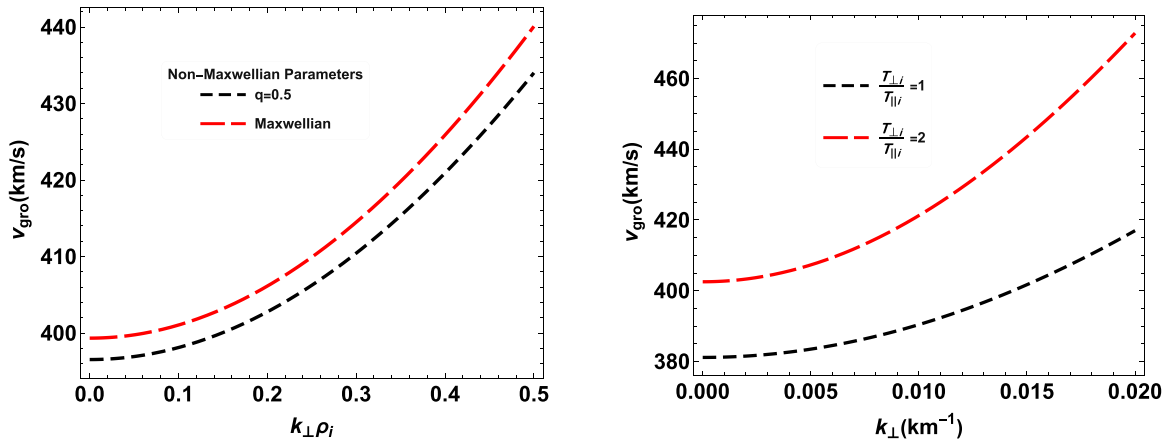

FIGURE 4
Group velocity of KAWs. The group velocity is calculated using Equation 10. In the left panel, $k_\perp$ is normalized with ρ_i. In the right panel, $T_{\perp i}$ varies, so $k_\perp$ is not normalized with ρ_i. The remaining quantities in both panels are the same as in Figure 1.

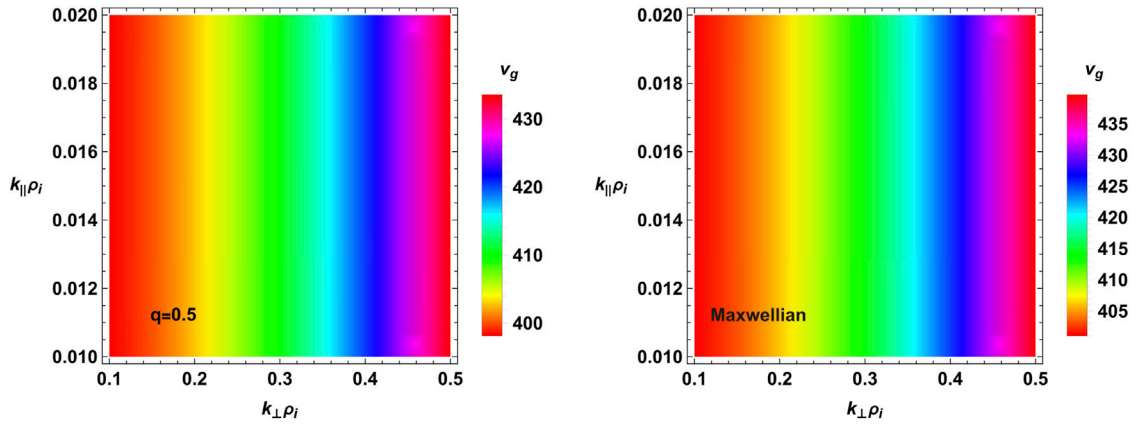

FIGURE 5
Effect of wavenumber on the group velocity of KAWs. The two panels are based on Equation 10. Both the perpendicular and parallel wavenumbers are normalized with ρ_i. The value of $q = 0.5$ in the left panel and $q \to 1$ in the right panel, and all other parameters are the same as in Figure 1. The bar legends right to both panels show the magnitude of the group velocity of the waves.

3 Results and discussion

For our analysis, we consider the propagation of the KAWs in the magnetopause where the plasma equilibrium density n_0 = 10 cm^{-3}, the background magnetic field B_0 = 55 nT, $T_{\|i}$ = 175 eV, $T_{\perp i}$ = 350 eV, and $T_{\|e} = T_{\perp e}$ = 35 eV, (Gershman et al., 2017). The 3-D global-scale hybrid simulation shows that S ~ 10^{-5} Wm^{-2} (Wang et al., 2019). These waves can strongly interact with the plasma. In the resonant process, physically, the velocities of the resonant electrons approach the phase velocity of the KAWs. Those electrons whose velocities are slightly below the phase velocity of the KAWs gain energy from the wave, in contrast to those electrons whose velocities are slightly above the phase velocity of the KAWs that give energy to the wave. The non-extensive distribution has a negative slope, thus, on average more particles take energy from the KAWs. During the resonant interaction, in the highly non-Maxwellian cases, the electrons gain more kinetic energy from waves (Figure 1). Moreover, the velocity of resonant electrons is ~ 1,000 km/s even after the waves cover a distance of 10 R_E.

Waves of different wavelengths can interact differently. When the perpendicular wavenumber of the waves is small, i.e., large perpendicular wavelength, then the particles are accelerated to higher velocities (Figure 2), and because the waves lose energy during their journey, energization takes place more efficiently near the regions where the waves are excited, as the magnitude of the velocity reduces (see bar legends in Figure 2). It can also be seen that the parallel wavenumber does not significantly influence the resonant velocity.

The particle energization takes place parallel to the background magnetic field. Consequently, a field-aligned beam of charged particles can be created. Such beams have been reported to exist very often in the magnetosphere (Song et al., 1993; Lee et al., 1994). The beams of the accelerated charged particles precipitate into the

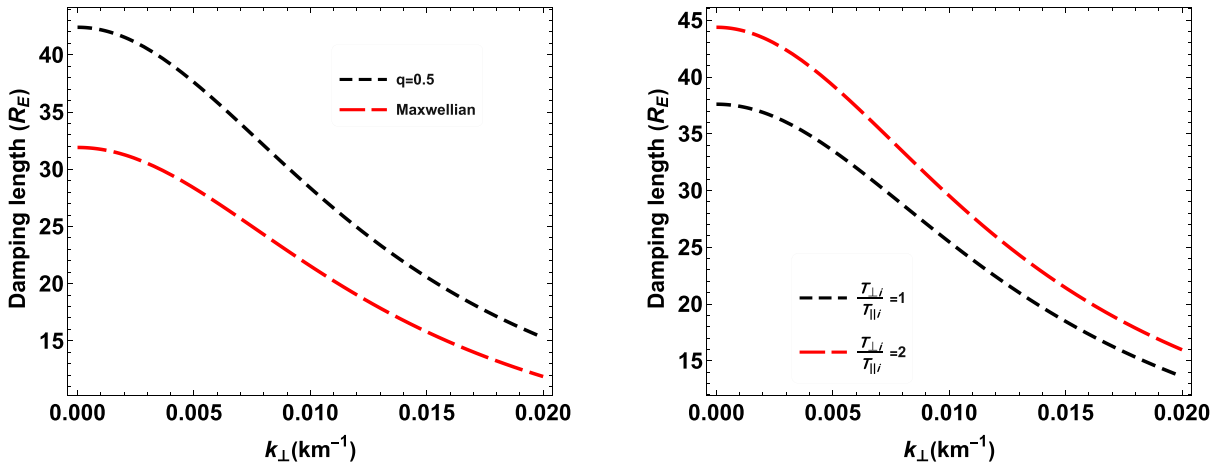

FIGURE 6
Damping length of KAWs. The damping length is calculated using Equation 11. In panels (left) and (right), we considered different values of the index q and $T_{\perp i}$. All other parameters are the same as in Figure 1.

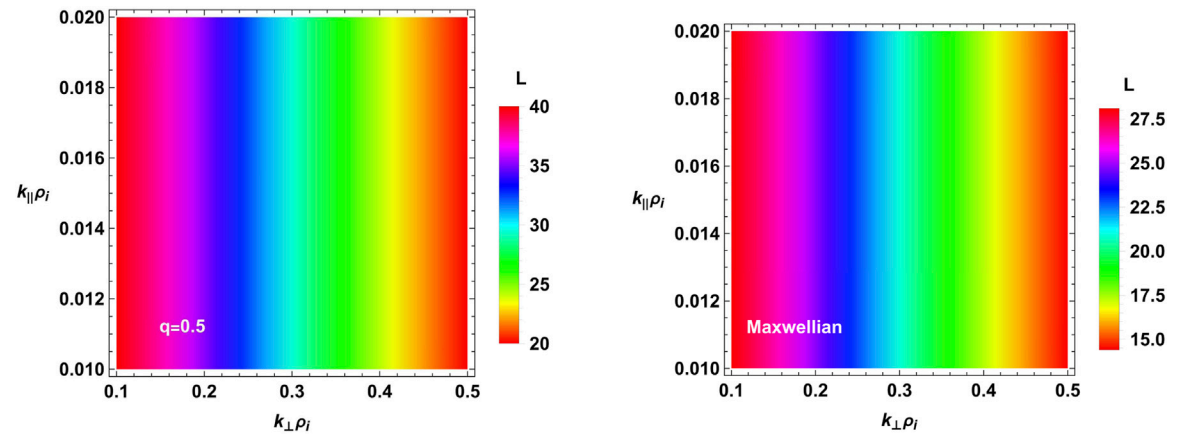

FIGURE 7
Effect of wavenumber on the damping length of KAWs. In the left and right panels, we considered $q = 0.5$ and $q \to 1$, respectively. The bar legends right to both panels represent the magnitude of the damping length of KAWs.

ionosphere (Skjæveland et al., 2017) and can play a vital role in the aurora formation (Chaston, 2006).

When the waves propagate toward the ionosphere, they carry field-aligned Poynting fluxes ~50 mWm^{-2} which are sufficient to drive aurora (Chaston et al., 2007). Waves having small perpendicular wavelengths damp out before reaching the ionosphere; however, this effect is balanced by other processes such as phase mixing, which continually regenerates KAWs of small perpendicular wavelengths (Lysak, 2023).

In some instances, the electron temperature remains isotropic, but the ion temperature is not (Gershman et al., 2017). When the perpendicular ion temperature increases, the wave interacts with the plasma such that resonant particles extract some of the wave's energy, resulting in comparatively low particle velocities (Figure 3).

When the waves propagate from regions where they are excited, the Poynting flux of the waves decreases with distance (Onishchenko et al., 2004). The rate at which this energy is transported can be obtained from the group velocity of KAWs. The group velocity, or the energy flow velocity, is larger for cases where the non-extensive parameter q and the perpendicular temperature $T_{\perp i}$ increase (Figure 4). That means that the hotter ions or Maxwellian distributed plasma permit the wave packets to propagate faster. The group velocity significantly increases in the perpendicular direction (Figure 5), which is consistent with the numerical simulations based on hybrid Vlasov-Maxwell model and Hall-magnetohydrodynamics (Pucci et al., 2016). In the magnetospheric plasmas, the variations in the group velocity significantly influence the propagation time of the waves from the onset sites (Lessard et al., 2006).

The waves that transport the energy are damped over a characteristic damping length larger than several R_E (Figure 6). The largeness of the damping length is not surprising as in the magnetosphere, the scale length varies from ~15 R_E to ~150 R_E (Lysak and Song, 2003). Our results show that the damping length

is larger when waves having large perpendicular wavelength (small $k_\perp$) travel in highly non-Maxwellian plasma ($q = 0.5$) where $T_{\perp i} > T_{\parallel i}$ (see Figures 6, 7). In the non-Maxwellian states ($q = 0.5$), the largeness of the damping length means that few resonant particles participate in the wave-particle interaction compared to the Maxwellian state. This causes a weak damping of the KAWs, which can interact with the charged particles over long distances.

The damping of the waves resulting in charged particle acceleration is Landau damping, and the waves are most likely to be caused by magnetic reconnection. As we have seen from Equation 1, the Landau damping is incorporated in the steady-state Poynting theorem, and there is strong evidence from kinetic particle-in-cell (PIC) P3D simulations that confirm that once the KAWs are generated and travel away from the X-line, they experience Landau damping (Sharma Pyakurel et al., 2018). Moreover, both the PIC P3D simulations and spacecraft observations show that the steady-state Poynting theorem is fulfilled near/at the X-line (Genestreti et al., 2018). In our study, we have seen that the wave amplitude due to Landau damping is suppressed over distance, and the same must happen over time as shown by numerical analysis (Chettri et al., 2025).

To summarize this paper, we highlighted that when KAWs accelerate the charged particles in the magnetosphere of Earth, the velocities of the charges vary with respect to distance (R_E). We see that the velocities are significantly influenced by the presence of the temperature anisotropic non-extensive distribution function. The accelerated charged particles are central to the formation of auroras. In addition to studying the charged particles' velocities, we also investigate the impact of the said distribution function on the damping length and group velocity of KAWs. These findings help us in understanding the energy levels of KAWs and the extent to which they can propagate within the Earth's magnetosphere. The results and findings of this manuscript are widely applicable to the solar wind and corona, where particles are typically out of thermal equilibrium. Therefore, to model such realistic plasma systems, we are confident that our results are highly relevant and directly applicable to these regions. It must be noted that in this paper, we followed the local kinetic theory (Lysak and Song, 2003). In this approach, the gradients in the density and background magnetic field are considered to be larger than the wavelength of the waves. In other words, we assumed a constant magnetic field and constant density. Our main focus was to understand the influence of temperature anisotropy and non-extensivity on the behavior of the waves on a local kinetic scale. The local, homogeneous approximation to the magnetospheric plasma is supported by observations (Svenes et al., 2008; Haaland et al., 2009). Considering the case where B_0 and n vary significantly would modify the quantitative values. However, we believe that the trends of these quantities reported in this study remain intact under reasonable background variations. A fully non-local calculation with radially varying $B_0(r)$ and $n(r)$ is left for future work and is beyond the scope of this manuscript.

Data availability statement

The original contributions presented in the study are included in the article/supplementary material, further inquiries can be directed to the corresponding authors.

Author contributions

IK: Conceptualization, Data curation, Formal Analysis, Funding acquisition, Investigation, Methodology, Project administration, Resources, Software, Supervision, Validation, Visualization, Writing – original draft, Writing – review and editing. SA: Conceptualization, Data curation, Formal Analysis, Funding acquisition, Investigation, Methodology, Project administration, Resources, Software, Supervision, Validation, Visualization, Writing – original draft, Writing – review and editing. MS: Formal Analysis, Investigation, Validation, Visualization, Writing – review and editing. TK: Formal Analysis, Investigation, Validation, Visualization, Writing – review and editing.

Funding

The author(s) declared that financial support was not received for this work and/or its publication.

Acknowledgements

The authors express their sincere gratitude to the Frontiers editorial board for their generous support and assistance.

Conflict of interest

The author(s) declared that this work was conducted in the absence of any commercial or financial relationships that could be construed as a potential conflict of interest.

Generative AI statement

The author(s) declared that generative AI was not used in the creation of this manuscript.

Any alternative text (alt text) provided alongside figures in this article has been generated by Frontiers with the support of artificial intelligence and reasonable efforts have been made to ensure accuracy, including review by the authors wherever possible. If you identify any issues, please contact us.

Publisher's note

References

Alfvén, H. (1942). Existence of electromagnetic-hydrodynamic waves. *Nature* 150, 405–406. doi:10.1038/150405d0

Atkinson, G. (1970). Auroral arcs: result of the interaction of a dynamic magnetosphere with the ionosphere. *J. Geophys. Res.* 75, 4746–4755. doi:10.1029/ja075i025p04746

Ayaz, S., Khan, I. A., Iqbal, Z., and Murtaza, G. (2020). Alfvén waves in temperature anisotropic cairns distributed plasma. *Commun. Theor. Phys.* 72, 035502. doi:10.1088/1572-9494/ab5fb3

Ayaz, S., Li, G., and Khan, I. A. (2024a). Solar coronal heating by kinetic alfvén waves. *Astrophysical J.* 970, 140. doi:10.3847/1538-4357/ad5bdc

Ayaz, S., Zank, G., Khan, I., Li, G., and Rivera, Y. J. (2024b). Alfvén waves in the solar corona: resonance velocity, damping length, and charged particles acceleration by kinetic alfvén waves. *Sci. Rep.* 14, 27275. doi:10.1038/s41598-024-77975-6

Ayaz, S., Zank, G. P., Khan, I. A., Li, G., and Rivera, Y. J. (2025a). A study of particle acceleration, heating, power deposition, and the damping length of kinetic alfvén waves in Non-maxwellian coronal plasma. *Astronomy Astrophysics* 694, A23. doi:10.1051/0004-6361/202452376

Ayaz, S., Zank, G. P., Khan, I. A., Rivera, Y. J., Shalchi, A., and Zhao, L.-L. (2025b). Solar coronal heating: role of kinetic and inertial alfvén waves in heating and charged particle acceleration. *Mon. Notices R. Astronomical Soc.* 540, 3583–3595. doi:10.1093/mnras/staf952

Bers, A. (1999). Note on group velocity and energy propagation (MIT plasma science and fusion center).

Borovsky, J. E., and Funsten, H. O. (2003). Mhd turbulence in the earth's plasma sheet: dynamics, dissipation, and driving. *J. Geophys. Res. Space Phys.* 108. doi:10.1029/2002ja009625

Chaston, C. (2006). Ulf waves and auroral electrons. *Magnetos. ULF Waves Synthesis New Directions* 169, 239. doi:10.1029/169GM16

Chaston, C., Wilber, M., Mozer, F., Fujimoto, M., Goldstein, M., Acuna, M., et al. (2007). Mode conversion and anomalous transport in kelvin-helmholtz vortices and kinetic alfvén waves at the earth's magnetopause. *Phys. Rev. Lett.* 99, 175004. doi:10.1103/PhysRevLett.99.175004

Chettri, M. K., Singh, H. D., Shrivastav, V., Singh, B., and Mukherjee, R. (2025). Damped kinetic alfvén waves in earth's magnetosheath: numerical simulations and mms observations. *arXiv Preprint arXiv:2512.09828*. doi:10.48550/arXiv.2512.09828

Christon, S., Mitchell, D., Williams, D., Frank, L., Huang, C., and Eastman, T. (1988). Energy spectra of plasma sheet ions and electrons from 50 ev/e to 1 mev during plasma temperature transitions. *J. Geophys. Res. Space Phys.* 93, 2562–2572. doi:10.1029/ja093ia04p02562

Christon, S., Williams, D., Mitchell, D., Huang, C., and Frank, L. (1991). Spectral characteristics of plasma sheet ion and electron populations during disturbed geomagnetic conditions. *J. Geophys. Res. Space Phys.* 96, 1–22. doi:10.1029/90ja01633

Cramer, N. F. (2011). *The physics of Alfvén waves*. John Wiley and Sons.

Crooker, N., Eastman, T., and Stiles, G. (1979). Observations of plasma depletion in the magnetosheath at the dayside magnetopause. *J. Geophys. Res. Space Phys.* 84, 869–874. doi:10.1029/ja084ia03p00869

Dai, L., Han, Y., Wang, C., Yao, S., Gonzalez, W., Duan, S., et al. (2023). Geoeffectiveness of interplanetary alfvén waves. i. magnetopause magnetic reconnection and directly driven substorms. *Astrophysical J.* 945, 47. doi:10.3847/1538-4357/acb267

Genestreti, K. J., Cassak, P. A., Varsani, A., Burch, J. L., Nakamura, R., and Wang, S. (2018). Assessing the time dependence of reconnection with poynting's theorem: mms observations. *Geophys. Res. Lett.* 45, 2886–2892. doi:10.1002/2017gl076808

Gershman, D. J., F-Viñas, A., Dorelli, J. C., Boardsen, S. A., Avanov, L. A., Bellan, P. M., et al. (2017). Wave-particle energy exchange directly observed in a kinetic alfvén-branch wave. *Nat. Communications* 8, 14719. doi:10.1038/ncomms14719

Haaland, S., Lybekk, B., Svenes, K., Pedersen, A., Förster, M., Vaith, H., et al. (2009). Plasma transport in the magnetotail lobes. *Ann. Geophys.* 27, 3577–3590. doi:10.5194/angeo-27-3577-2009

Hasegawa, A., and Chen, L. (1975). Kinetic process of plasma heating due to alfvén wave excitation. *Phys. Rev. Lett.* 35, 370–373. doi:10.1103/physrevlett.35.370

Keiling, A. (2024). Alfvén waves across heliophysics: progress, challenges, and opportunities.

Khan, I. A., Iqbal, Z., and Murtaza, G. (2019a). Perturbed electromagnetic field and poynting flux of kinetic alfvén waves in kappa distributed space plasmas. *Eur. Phys. J. Plus* 134, 80. doi:10.1140/epjp/i2019-12487-3

Khan, I. A., Khokhar, T. H., Shah, H., and Murtaza, G. (2019b). Distinct features of alfvén wave in non-extensive plasmas. *Phys. A Stat. Mech. Its Appl.* 535, 122385. doi:10.1016/j.physa.2019.122385

Khan, I. A., Iqbal, Z., and Murtaza, G. (2020). Solar coronal heating by alfvén waves in bi-kappa distributed plasma. *Mon. Notices R. Astronomical Soc.* 491, 2403–2412. doi:10.1093/mnras/stz3178

Kirpichev, I., Antonova, E., and Znatkova, S. (2015). Evolution of spectral index of energetic protons in the magnetopause crossing at the subsolar point. *Geomagnetism Aeronomy* 55, 709–714. doi:10.1134/s0016793215060055

Kletzing, C., Scudder, J., Dors, E., and Curto, C. (2003). Auroral source region: plasma properties of the high-latitude plasma sheet. *J. Geophys. Res. Space Phys.* 108. doi:10.1029/2002ja009678

Kolmogorov, A. N. (1941). *Dissipation of energy in the locally isotropic turbulence*. London: The Royal Society, 19–21.

Lee, L., Johnson, J. R., and Ma, Z. (1994). Kinetic alfvén waves as a source of plasma transport at the dayside magnetopause. *J. Geophys. Res. Space Phys.* 99, 17405–17411. doi:10.1029/94ja01095

Lessard, M., Lund, E., Jones, S., Arnoldy, R., Posch, J., Engebretson, M., et al. (2006). Nature of pi1b pulsations as inferred from ground and satellite observations. *Geophys. Res. Lett.* 33. doi:10.1029/2006gl026411

Liu, Y., Wang, Y., and Hu, T. (2016). Dispersive alfvén waves in a plasma with anisotropic superthermal particles. *Phys. Plasmas* 23. doi:10.1063/1.4945635

Lu, J., Rankin, R., Marchand, R., Rae, I., Wang, W., Solomon, S., et al. (2007). Electrodynamics of magnetosphere-ionosphere coupling and feedback on magnetospheric field line resonances. *J. Geophys. Res. Space Phys.* 112. doi:10.1029/2006ja012195

Lysak, R. (2023). Kinetic alfvén waves and auroral particle acceleration: a review. *Rev. Mod. Plasma Phys.* 7 (6), 6. doi:10.1007/s41614-022-00111-2

Lysak, R. L., and Song, Y. (2003). Kinetic theory of the alfvén wave acceleration of auroral electrons. *J. Geophys. Res. Space Phys.* 108. doi:10.1029/2002JA009406

Lysak, R. L., and Song, Y. (2011). Development of parallel electric fields at the plasma sheet boundary layer. *J. Geophys. Res. Space Phys.* 116. doi:10.1029/2010ja016424

Mandt, M., and Lee, L. (1991). Generation of pc 1 waves by the ion temperature anisotropy associated with fast shocks caused by sudden impulses. *J. Geophys. Res. Space Phys.* 96, 17897–17901. doi:10.1029/91ja01733

Miura, A., and Sato, T. (1980). Numerical simulation of global formation of auroral arcs. *J. Geophys. Res. Space Phys.* 85, 73–91. doi:10.1029/ja085ia01p00073

Olbert, S. (1968). "Summary of experimental results from mit detector on imp-1," in *Physics of the magnetosphere: based upon the proceedings of the conference held at Boston College June 19–28, 1967* (Springer), 641–659.

Olson, J. V., and Lee, L. (1983). Pc1 wave generation by sudden impulses. *Planet. Space Sci.* 31, 295–302. doi:10.1016/0032-0633(83)90079-x

Onishchenko, O., Pokhotelov, O., Sagdeev, R., Stenflo, L., Treumann, R., and Balikhin, M. (2004). Generation of convective cells by kinetic alfvén waves in the upper ionosphere. *J. Geophys. Res. Space Phys.* 109. doi:10.1029/2003JA010248

Pollock, C. J., Burch, J. L., Chasapis, A., Giles, B. L., Mackler, D. A., Matthaeus, W. H., et al. (2018). Magnetospheric multiscale observations of turbulent magnetic and electron velocity fluctuations in earth's magnetosheath downstream of a quasi-parallel bow shock. *J. Atmos. Solar-Terrestrial Phys.* 177, 84–91. doi:10.1016/j.jastp.2017.12.006

Pucci, F., Vasconez, C. L., Pezzi, O., Servidio, S., Valentini, F., Matthaeus, W. H., et al. (2016). From alfvén waves to kinetic alfvén waves in an inhomogeneous equilibrium structure. *J. Geophys. Res. Space Phys.* 121, 1024–1045. doi:10.1002/2015ja022216

Qiu, H.-B., and Liu, S.-B. (2013). Weibel instability with nonextensive distribution. *Phys. Plasmas* 20, 102119. doi:10.1063/1.4826447

Shamir, M., Khan, I. A., and Murtaza, G. (2022). Charged particles energization during magnetic reconnection in the earth's magnetosphere by double layers: an analytical approach. *Mon. Notices R. Astronomical Soc.* 509, 3703–3708. doi:10.1093/mnras/stab3236

Sharma Pyakurel, P., Shay, M. A., Haggerty, C. C., Parashar, T., Drake, J. F., Cassak, P., et al. (2018). Super-alfvénic propagation and damping of reconnection onset signatures. *J. Geophys. Res. Space Phys.* 123, 341–349. doi:10.1002/2017JA024606

Shay, M., Drake, J., Eastwood, J., and Phan, T. (2011). Super-alfvénic propagation of substorm reconnection signatures and poynting flux. *Phys. Review Letters* 107, 065001. doi:10.1103/PhysRevLett.107.065001

Skjæveland, Å. S., Carlson, H. C., and Moen, J. I. (2017). A statistical survey of heat input parameters into the cusp thermosphere. *J. Geophys. Res. Space Phys.* 122, 9622–9651. doi:10.1002/2016ja023594

Song, P., Russell, C., Fitzenreiter, R., Gosling, J., Thomsen, M., Mitchell, D., et al. (1993). Structure and properties of the subsolar magnetopause for northward interplanetary magnetic field: multiple-instrument particle observations. *J. Geophys. Res. Space Phys.* 98, 11319–11337. doi:10.1029/93ja00606

Streltsov, A., and Lotko, W. (2004). Multiscale electrodynamics of the ionosphere-magnetosphere system. *J. Geophys. Res. Space Phys.* 109. doi:10.1029/2004ja010457

Summers, D., Xue, S., and Thorne, R. M. (1994). Calculation of the dielectric tensor for a generalized lorentzian (kappa) distribution function. *Phys. Plasmas* 1, 2012–2025. doi:10.1063/1.870656

Svenes, K., Lybekk, B., Pedersen, A., and Haaland, S. (2008). Cluster observations of near-earth magnetospheric lobe plasma densities–a statistical study. *Ann. Geophys.* 26, 2845–2852. doi:10.5194/angeo-26-2845-2008

Tang, X., Cattell, C., Dombeck, J., Dai, L., Wilson III, L. B., Breneman, A., et al. (2013). Themis observations of the magnetopause electron diffusion region: large amplitude waves and heated electrons. *Geophys. Res. Lett.* 40, 2884–2890. doi:10.1002/grl.50565

Tiwari, B., Mishra, R., Varma, P., and Tiwari, M. (2008). Shear-driven kinetic alfven wave in the plasma sheet boundary layer. *Earth, Planets Space* 60, 191–205. doi:10.1186/bf03352782

Tsallis, C. (1988). Possible generalization of boltzmann-gibbs statistics. *J. Statistical Phys.* 52, 479–487. doi:10.1007/bf01016429

Vasyliunas, V. M. (1968). Low-energy electrons on the day side of the magnetosphere. *J. Geophys. Res.* 73, 7519–7523. doi:10.1029/ja073i023p07519

Walker, A. D. M. (2013). *Plasma waves in the magnetosphere*. Springer Science and Business Media.

Wang, X., Liu, Z., Li, Z., and Zhang, X. (1998). Kinetic alfven waves driven by velocity shear. *Phys. Plasmas* 5, 836–840. doi:10.1063/1.872650

Wang, H., Lin, Y., Wang, X., and Guo, Z. (2019). Generation of kinetic alfvén waves in dayside magnetopause reconnection: a 3-d global-scale hybrid simulation. *Phys. Plasmas* 26. doi:10.1063/1.5092561

Watanabe, T.-H. (2014). A unified model of auroral arc growth and electron acceleration in the magnetosphere-ionosphere coupling. *Geophys. Res. Lett.* 41, 6071–6077. doi:10.1002/2014gl061166

Wright, A. N., Hartinger, M. D., Takahashi, K., and Elsden, T. (2024). Alfven waves in the earth's magnetosphere. Alfvén waves across heliophysics: progress, challenges, and opportunities. 215–247.

Wu, D.-J., and Chen, L. (2020). Kinetic alfvén waves in laboratory, space, and astrophysical plasmas.

Wygant, J., Keiling, A., Cattell, C., Lysak, R., Temerin, M., Mozer, F., et al. (2002). Evidence for kinetic alfvén waves and parallel electron energization at 4–6 re altitudes in the plasma sheet boundary layer. *J. Geophys. Res. Space Phys.* 107, SMP–24. doi:10.1063/1.5092561

Xunaira, S., Khan, I. A., Shamir, M., Iqbal, Z., and Murtaza, G. (2023). Instability and energy transport of kinetic alfvén waves in the solar corona. *Eur. Phys. J. Plus* 138, 1–10. doi:10.1140/epjp/s13360-023-04352-z